archives
of thermodynamics
Vol. **41**(2020), No. 1, 3–30
DOI: 10.24425/ather.2020.132948

Numerical investigation and sensitivity analysis of turbulent heat transfer and pressure drop of Al_2O_3/H_2O nanofluid in straight pipe using response surface methodology

OLATOMIDE G. FADODUN *[a]
ADEBIMPE A. AMOSUN[a]
AYODEJI O. SALAU[b]
DAVID O. OLALOYE [a]
JOHNSON A. OGUNDEJI[a]
FRANCIS I. IBITOYE[a]
FATAI A. BALOGUN[a]

[a] Department of Physics, Obafemi Awolowo University, Ile-Ife, Osun state. P.M.B. 13, Ile-Ife, Osun, 220282 Nigeria.

[b] Department of Electrical/Electronic and Computer Engineering, Afe Babalola University, Ado-Ekiti, Nigeria

Abstract In this paper, investigation of the effect of Reynolds number, nanoparticle volume ratio, nanoparticle diameter and entrance temperature on the convective heat transfer and pressure drop of Al_2O_3/H_2O nanofluid in turbulent flow through a straight pipe was carried out. The study employed a computational fluid dynamic approach using single-phase model and response surface methodology for the design of experiment. The Reynolds average Navier-Stokes equations and energy equation were solved using k-ε turbulent model. The central composite design method was used for the response-surface-methodology. Based on the number of variables and levels, the condition of 30 runs was defined and 30 simulations were performed. New models to evaluate the mean Nusselt number and pressure drop were obtained. Also, the result showed that all the four input variables are statistically significant to the pressure drop while three out of them are significant

*Corresponding Author. Email: ofadodun@cerd.gov.ng

to the Nusslet number. Furthermore, sensitivity analysis carried out showed that the Reynolds number and volume fraction have a positive sensitivity to both the mean Nusselt number, and pressure drop, while the entrance temperature has negative sensitivities to both.

Keywords: Nusselt number; Reynolds number; Pressure drop; Response-surface-methodology; Nanofluid; Single-phase flow

Nomenclature

C_μ	–	turbulent constant
$C_{1\varepsilon}$, $C_{2\varepsilon}$	–	turbulent constant
c_p	–	specific heat capacity at constant pressure, J/kgK
D_h	–	diameter of the pipe, m
d	–	diameter of the nanoparticle, m
f	–	friction factor
G_k	–	rate of production of turbulent kinetic energy, J/kg
h	–	coefficent of heat transfer, W/m^{2}K
I	–	turbulence intensity
k	–	turbulence kinetic energy, m^2/s^2
Nu	–	Nusselt number
T	–	temperature of base fluid, K
Pr	–	Prandtl number of base fluid
Δp	–	pressure drop
q''	–	heat flux at the surface of the pipe
R^2	–	coefficient of determination
Re	–	Reynolds number
Re$_p$	–	nanoparticle Reynolds number
r	–	radial distance, m
S	–	modulus of rate of strain tensor
u_r, u_x	–	components velocity, m/s
x	–	axial distance, m
y^+	–	nondimensionalized wall normal distance

Greek symbols

α	–	thermal diffusivity, m^2/s
ε	–	turbulence energy dissipation, m^2/s^3
λ	–	thermal conductivity, W/m K
μ	–	dynamic viscosity, kg/m s
ρ	–	density of base fluid, kg/m^3
σ_k, σ_t, σ_ε	–	turbulent constant
φ	–	nanoparticle volume fraction

Subscripts

in	–	inlet
nf	–	nanofluid
p	–	nanoparticle
f	–	base fluid
fr	–	freezing point
t	–	turbulent

Abbreviations

RSM	–	response surface methodology
MWCNT	–	multiwall carbon nanotube
SWCNT	–	single-wall carbon nanotube

1 Introduction

Nanofluid belongs to a class of heat transport fluids formed by the dilute suspension of a small amount of metallic or non-metallic nanoparticles in a base fluid. These hybrid materials have high thermal conductivities and are considered to be the next-generation heat transfer fluids. The concept was first proposed by Choi in 1995 at the Argon National Laboratory when he conducted an experiment on a nanofluid and reported enhancements in its thermal conductivity as compared to the base fluid [1]. Other researchers like Eastman [2] and Wang *et al.*, [3] worked on Al_2O_3/H_2O and Cu/Ethylene glycol (EG) and reported increment of 30% and 40% in the thermal conductivities respectively.

Experimental investigations have shown that the enhancement observed in the thermal conductivity of a nanofluid depends on several parameters such as particle volume fraction, size of the nanoparticle, shape of the nanoparticle, nanoparticle clustering, Brownian motion of nanoparticle in the base fluid, temperature and thermophysical properties of the base fluid and nanoparticle [4].

Convective heat transfer in a nanofluid for both laminar and turbulent flow regimes have been studied by several scientists. Sharma *et al.* [5] investigated the convective heat transfer coefficient and friction factor of Al_2O_3/H_2O nanofluid in the circular straight pipe with a twisted coil inserted under the turbulent regime. The results revealed an increment of 27.3% and 24% in heat transfer coefficient and friction factor respectively. Chandrasekar *et al.* [6] investigated CuO /water/propylene glycol nanofluid in a straight horizontal circular tube with and without a helical coil inserted for a range of Reynolds number spanning laminar to turbulent regimes. They reported a 28% increase in the Nusselt number and a 10% increase

in the friction factor compared to the base fluid. Li & Xuan [7] investigated the effect of Reynolds number and volume ratio on the convective heat transfer and friction factor using Cu/H_2O nanofluid flowing through a straight pipe. The convective heat transfer was reported to have an increment of about 60% for a 2% volume ratio while the friction factor was only slightly enhanced.

Convective heat transfer in a nanofluid has also been studied numerically using computational fluid dynamics in conjunction with models that described the thermophysical properties of the nanofluid. Two popular models used are the single-phase and two-phase discrete (Eulerian-Langrangian) model. The single phase model treats the nanofluid as a unique fluid without considering the interaction between the fluid and the nanoparticles while the other considers the interaction between the fluid and the nanoparticle [8]. Saha [9] numerically studied the heat transfer and entropy generation in the turbulent regime in TiO_2/H_2O nanofluid flowing in a straight horizontal circular pipe using both single and two-phase mixture models. The study investigated the effect of Reynolds number, volume ratio and nanoparticle diameter on the heat transfer rate and entropy generation. The result showed that convective heat transfer and entropy generation increase as the volume ratio and Reynolds number increase and decrease respectively with increasing size of the nanoparticle. Safaei *et al.* [10] studied the heat transfer coefficient, friction loss, pressure drop and pumping power needed for graphene/nanoplatelets/silver/water based nanofluid in a rectangular duct under the turbulent regime. The authors reported an increase in the heat transfer coefficient as the nanosheet concentration and Reynolds number increased. However, as a direct consequence of the increment, there was also an increase in pressure drop and pumping power. Hussein *et al.* [11] studied the effect of Reynolds number and volume fraction on convective heat transfer and friction factor of TiO_2/H_2O nanofluid flowing through a horizontal tube with constant heat flux under a turbulent regime using the single-phase model. The result obtained showed that both the friction factor and heat transfer coefficient were enhanced by an increase in the concentration of TiO_2 and Reynolds number. Fadodun *et al.* [12] investigated thermal efficiency and pumping power of nanofluid flowing through a pipe in turbulent flow regime using computational fluid dynamic and response surface methodology. The study considered the effect of Reynolds number, nanoparticle volume fraction, nanoparticle size and entrance temperature on thermodynamic second law efficiency and pumping power. The authors

reported that all four input variables are statistically significant to both thermal efficiency and pumping power. Also, sensitivity analysis carried out on the regression model obtained showed that the Reynolds number is the most sensitive parameter to both the thermal efficiency and loss in pumping power. Also, Fadodun *et al.* [13] investigated the effect of Reynolds number and nanoparticle volume ratio on thermal performance of SWCNT (single wall carbon nanotube) nanofluid flowing through a pipe in turbulent flow regime. The result was presented in terms of entropy production, second thermodynamic efficiency, Nusselt number, pressure drop, Bejan number and entropy generation number. The result revealed that SWCNT nanofluid is only beneficial at low Reynolds numbers. Chan *et al.* [14] investigated heat transfer in Al_2O_3/H_2O bionanofluid flowing through a pipe with constant wall temperature using single and two-phase mixture models. Analysis of the data obtained from both models showed close similarities when compared with the experimental result. Albojamal *et al.* [15] studied convective heat transfer and pressure drop in nanofluid under constant heat flux and constant temperature boundary condition using a single-phase model with temperature-dependent thermophysical properties and two-phase discrete model. Their results showed that the two models were in good agreement with experimental values. This further reinforced the fact that the single phase model can provide a reliable fast and low-cost method of investigating convective heat transfer in nanofluids.

In recent times researchers have introduced response surface methodology analysis to get a better understanding of the convective heat transfer processes, as many of the earlier studies were carried out based on investigations of one factor at a time [16]. This failed to capture the effects of the interactions between the input variables on the dependent variables. Mamourian *et al.* [17] investigated the effect of Reynolds number, nanoparticle volume fraction, nanoparticle size on the average Nusselt number using numerical approach and response surface methodology (RSM). Wen *et al.* [18] studied the effect of temperature and velocity of nanofluid flowing through a pipe on two dependent variables – mean Nusselt and Reynolds numbers – using response surface methodology. Their results showed that both the input variables and the interactions between them were significant to the dependent variables. Shanbedi *et al.* [19] studied experimentally the effect of three input variables – nanoparticle volume fraction, flow rate and magnetic field – on heat transfer in a multiwall carbon nanotube (MWCNT) deionized water nanofluid in a straight horizontal circular pipe under the

influence of a magnetic field. The optimization of the experiment was done using RSM. The optimized values for the three variables (volume fraction, flow rate and magnetic flux) were given as 0.09%, 301.3 ml/min and 400 G, respectively. The experiment was conducted at these values and the result obtained was in agreement with one proposed by RSM. Finally, Konchada *et al.* [20] studied the effect of entrance temperature and mass flow rate on entropy generation of Al_2O_3/H_2O nanofluid flowing through a longitudinal fin heat exchanger using computational fluid dynamics and Taguchi technique. The result of ANOVA (analysis of variance) showed that both inlet temperature and mass flow rate are statistically significant to the entropy generation but the effect of inlet temperature is the most profound between the two.

As so far observed, it can be deduced that majority of the works carried out by several authors involved the use of RSM in their study of convective heat transfer in nanofluids and considered two or three factors at a time. So far, to the best of our knowledge, perhaps only a few or no author at all has considered the effect of entrance temperature in the evaluation of convective heat transfer of a nanofluid. Furthermore, most of the works already reported have focused mainly on the laminar flow regime. Thus, the motivation for this study is a comprehensive investigation of the effect of four input parameters – Reynold number, nanoparticle volume ratio, nanoparticle size and entrance temperature – on pressure drop and convective heat transfer of Al_2O_3/H_2O nanofluid in a turbulent flow through a pipe. The study employed a computational fluid dynamic approach using single phase approximation and response surface methodology for the design of the experiment.

2 Problem statement

The problem under investigation involves the steady state turbulent forced convection of Al_2O_3/H_2O nanofluid flowing through a horizontal pipe, Fig. 1. The geometry composes of diameter 0.02 m and length 2 m, the fluid enters the pipe with uniform velocity and temperature. A constant heat flux of 1000 W/m^2 was applied to the wall of the pipe and zero pressure gauge was assumed at the outlet. The flow and the temperature fields are assumed to be symmetrical about the tube's main axis. Thus a 2D axisymmetric formulation is employed to simplify the problem.

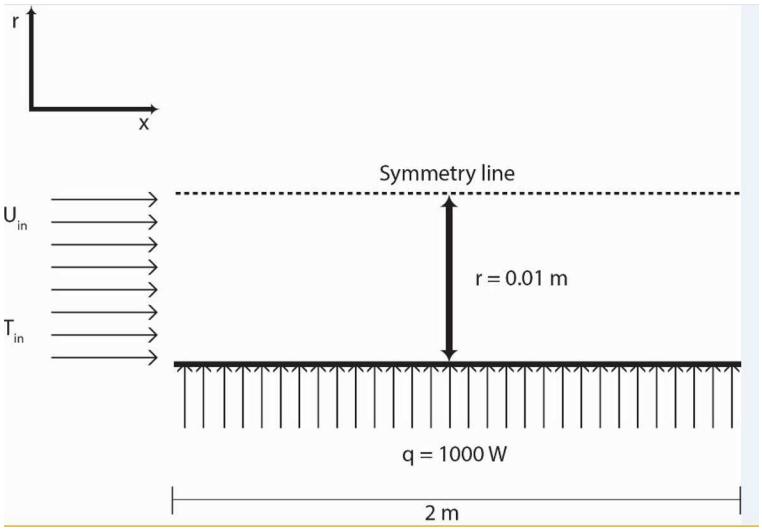

Figure 1: Geometry of the problem.

2.1 Single-phase model

This model assumes the nanoparticle dispersed in the base fluid is fluidized, and the resulting suspension can hence be treated as a single phase fluid. Both the nanoparticle and base fluid are in thermal equilibrium with no slip between them and the thermophysical properties depend on the properties of the base fluid and nanoparticle [21,22]. As a result, the governing equations (continuity, momentum, and energy) applied to the classical Newtonian fluid is also valid for this model. The model assumes the nanofluid is incompressible, neglecting viscous and compressive work in the energy equation. Therefore, the hydrodynamic and heat transfer equations take the forms [21]:

$$\nabla \bar{u} = \frac{\partial u_x}{\partial x} + \frac{\partial u_r}{\partial r} + \frac{u_r}{r} = 0 \,, \tag{1}$$

$$\begin{aligned} u_x \frac{\partial u_x}{\partial x} + u_r \frac{\partial u_x}{\partial r} \quad = \quad & -\frac{1}{\rho_{nf}} \frac{\partial p}{\partial x} + \frac{1}{\rho_{nf}} \frac{1}{r} \frac{\partial}{\partial r} \left[r \left(\mu_{nf} + \mu_t \right) \frac{\partial u_x}{\partial r} \right] \\ & + \frac{1}{\rho_{nf}} \frac{\partial}{\partial x} \left[\left(\mu_{nf} + \mu_t \right) \frac{\partial u_x}{\partial x} \right] \,, \end{aligned} \tag{2}$$

$$u_r\frac{\partial u_r}{\partial r} + u_x\frac{\partial u_r}{\partial x} = -\frac{1}{\rho_{nf}}\frac{\partial p}{\partial r} + \frac{1}{\rho_{nf}}\frac{1}{r}\frac{\partial}{\partial r}\left[r\left(\mu_{nf}+\mu_t\right)\frac{\partial u_r}{\partial r}\right] + \frac{1}{\rho_{nf}}\frac{\partial}{\partial x}\left[\left(\mu_{nf}+\mu_t\right)\frac{\partial u_r}{\partial x}\right] - \frac{1}{\rho_{nf}}\frac{u_r}{r^2}\left(\mu_{nf}+\mu_t\right)\,, \tag{3}$$

$$u_x\frac{\partial T_{nf}}{\partial x} + u_r\frac{\partial T_{nf}}{\partial r} = \frac{1}{r}\frac{\partial}{\partial r}r\left(\alpha_{nf}+\alpha_t\right)\frac{\partial T_{nf}}{\partial r} + \frac{\partial}{\partial x}\left(\alpha_{nf}+\alpha_t\right)\frac{\partial T_{nf}}{\partial x}\,, \tag{4}$$

where μ_t, α_{nf}, and α_t are turbulence viscosity, thermal diffusivity of the nanofluid and turbulence diffusivity, respectively. The turbulence viscosity and diffusivity are expressed in equations:

$$\mu_t = C_\mu\rho\frac{k^2}{\varepsilon}\,, \tag{5}$$

$$\alpha_t = \frac{\mu_t}{\rho_{nf}\sigma_t}\,, \tag{6}$$

where σ_t and C_μ are constants.

In terms of turbulent motion, the last term on the RHS of Eq. (2) is small and thus reduced to

$$u_x\frac{\partial u_x}{\partial x} + u_r\frac{\partial u_x}{\partial r} = -\frac{1}{\rho_{nf}}\frac{\partial p}{\partial x} + \frac{1}{\rho_{nf}}\frac{1}{r}\frac{\partial}{\partial r}\left[r\left(\mu_{nf}+\mu_t\right)\frac{\partial u_x}{\partial r}\right]\,. \tag{7}$$

Also in turbulent motion, the advection term, i.e. the last term on the RHS is negligibly small and thus Eq. (4) is reduced to

$$u_x\frac{\partial T_{nf}}{\partial x} + u_r\frac{\partial T_{nf}}{\partial r} = \frac{1}{r}\frac{\partial}{\partial r}r\left(\alpha_{nf}+\alpha_t\right)\frac{\partial T_{nf}}{\partial r}\,. \tag{8}$$

Using the standard k-ε turbulent model, the equations for turbulent kinetic energy, k, and dissipation rate, ε, are given as [23]:

$$\frac{1}{r}u_r\frac{\partial}{\partial r}\left(rk\right) + u_x\frac{\partial k}{\partial x} = \frac{1}{\rho_{nf}}\frac{1}{r}\frac{\partial}{\partial r}\left[r\left(\mu_{nf}+\frac{\mu_t}{\sigma_k}\right)\right]\frac{\partial k}{\partial r} + \frac{1}{\rho_{nf}}\frac{\partial}{\partial x}\left[\left(\mu_{nf}+\frac{\mu_t}{\sigma_k}\right)\frac{\partial k}{\partial x}\right] + G_k - \rho\varepsilon\,, \tag{9}$$

$$\frac{1}{r}u_r\frac{\partial}{\partial r}\left(r\varepsilon\right) + u_x\frac{\partial \varepsilon}{\partial x} = \frac{1}{\rho}\frac{1}{r}\frac{\partial}{\partial r}\left[r\left(\mu_{nf}+\frac{\mu_t}{\sigma_\varepsilon}\right)\right]\frac{\partial \varepsilon}{\partial r} + \frac{1}{\rho_{nf}}\frac{\partial}{\partial x}\left[\left(\mu_{nf}+\frac{\mu_t}{\sigma_\varepsilon}\right)\frac{\partial k}{\partial x}\right] + G_k C_{1\varepsilon}\frac{\varepsilon}{k} - C_{2\varepsilon}\rho_{nf}\frac{\varepsilon^2}{k}\,, \tag{10}$$

where G_k is the rate of production of turbulent kinetic energy given as

$$G_k = \mu_t S^2 \ , \tag{11}$$

where $S = \sqrt{2S_{ij}S_{ij}}$ is the modulus of the rate of strain tensor. Values of the constants used are given in Tab. 1.

Table 1: Values of constants used in k-ε turbulent model.

Constant	$C_{1\varepsilon}$	$C_{2\varepsilon}$	C_μ	σ_k	σ_ε	σ_t	Von Karman
Value	1.44	1.92	0.09	1.0	1.3	0.9	0.4

The inlet turbulence intensity is calculated using the relation

$$I = 0.16\mathrm{Re}^{-\frac{1}{8}} \ . \tag{12}$$

The Reynolds number and Darcy friction factor for turbulent flow are defined as:

$$\mathrm{Re} = \frac{\rho D_h u_{mean}}{\mu} \ , \tag{13}$$

$$f = \frac{2D_h \Delta p}{\rho u_{mean}^2 H} \ , \tag{14}$$

where D_h is the diameter of the pipe, while H is the length of the pipe, and the mean velocity u_{mean} is defined as

$$u_{mean} = \frac{2}{R^2}\int_0^R u\left(x,r\right)\, r dr \ . \tag{15}$$

The heat transfer coefficient is defined as

$$h\left(x\right) = \frac{q''}{T_{wall} - T_{bulk}}, \tag{16}$$

where q'' is the heat flux at the surface of the pipe, and

$$T_{bulk}\left(x\right) = T\left(x_0\right) + \frac{q''\pi D_h x}{\dot{m}c_p} \ , \tag{17}$$

where $T\left(x_0\right)$ is the mean temperature at the point, x_0, where the flow is fully developed. Here x_0 is taken as $70D_h = 1.4$ m from the entrance

length.

The Nusselt number is defined as

$$Nu(x) = \frac{h(x)D}{k} \, . \tag{18}$$

The mean Nusselt number is evaluated using Simpson's 1/3 rule given as

$$\mathrm{Nu}_{ave} = \frac{1}{x_{out} - x_{in}} \int_{x_{in}}^{x_{out}} \mathrm{Nu}(x) dx \, . \tag{19}$$

Note that the initial point, x_{in}, is taken as 1.4 m. At this point, the flow is assumed to be fully developed while $x_{out} = 2$ m.

2.2 Boundary conditions

Inlet

$$u_x = u_o \, , \quad u_r = 0 \, , \quad T = T_o \, , \quad k = \frac{3}{2} \left(I \bar{u} \right)^2 , \quad \varepsilon = \frac{c_\mu^{0.75} k^{1.5}}{L} \, . \tag{20}$$

Here $\bar{u}$ is the velocity scale which is equivalent to the inlet velocity u_o, L is the turbulence length scale, which is taken as the diameter of the pipe and I is the turbulence intensity given by Eq. (10).

Outlet

Parameters u_x, u_r, k, ε, and T were assumed to be fully developed and the static gauge pressure is taken as 0

$$\frac{\partial u_r}{\partial x} = \frac{\partial u_x}{\partial x} = \frac{\partial T}{\partial x} = \frac{dk}{dx} = \frac{d\varepsilon}{dx} = 0 \, , \quad p_{gauge} = 0 \, . \tag{21}$$

Wall

No-slip condition constraint is invoked

$$u_x = 0 \, , \quad u_r = 0 \, , \quad \varepsilon = 0 \, , \quad q = 1000 \ \ \mathrm{W/m^2} \, . \tag{22}$$

Symmetry line

$$\frac{\partial u_r}{\partial r} = 0, \quad \frac{\partial T}{\partial r} = 0 \, . \tag{23}$$

Thermophysical properties of water

The density, viscosity, heat capacity and thermal conductivity of water in terms of temperature as proposed by Kays *et al.* [24] is used in this study:

$$\rho_f = 330.12 + 5.92T - 1.63 \times 10^{-2}T^2 + 1.33 \times 10^{-5}T^3 \,, \tag{24}$$

$$c_p = 10^{-3}\left(10.01 - 5.14 \times 10^{-2}T + 1.49 \times 10^{-4}T^2 - 1.43 \times 10^{-7}T^3\right) \,, \tag{25}$$

$$\mu_f = 0.00002414 \times 10^{\left(\frac{247.81}{T-140}\right)} \,, \tag{26}$$

$$k_f = 0.76761 + 7.53211 \times 10^{-3}T - 0.98244 \times 10^{-5}T^2 \,. \tag{27}$$

Using a single-phase model, the density and specific heat of the nanofluid were estimated using the relations [25]:

$$\rho_{nf} = (1-\varphi)\,\rho_{bf} + \varphi\rho_{np} \,, \tag{28}$$

$$C_{pnf} = \frac{(1-\varphi)\,(\rho C_p)_{bf} + \varphi\,(\rho C_p)_{np}}{\rho_{nf}} \,, \tag{29}$$

where ρ_{bf} is the density of the base fluid which is water in this work.

Corcione empirical formulas were used to estimate the thermal conductivity and viscosity of the nanofluid [26]:

$$\frac{\mu_f}{\mu_{nf}} = 1 - 34.87\left(\frac{d_p}{d_f}\right)^{-0.3}\varphi^{1.03} \,, \tag{30}$$

$$\frac{k_{nf}}{k_f} = 1 + 4.4\mathrm{Re}_p^{0.4}\mathrm{Pr}_f^{0.66}\left(\frac{T_{nf}}{T_{fr}}\right)^{10}\left(\frac{k_{np}}{k_f}\right)^{0.33}\varphi^{0.66} \,, \tag{31}$$

where $d_f = 0.1\left(\frac{6M}{N\pi\rho_f}\right)$ and $\mathrm{Re}_p = \frac{2\rho_f K_b T_{nf}}{\pi\mu_f^2 d_p}$.

To obtain the thermophysical properties of nanofluid using single phase model, the thermophysical properties of water were first evaluated at a range of entrance temperature considered using Eqs. (22)–(25). The values obtained were used with the thermophysical properties of bulk Al_2O_3 shown in Tab. 2 to estimate the thermophysical properties of Al_2O_3 nanofluid using Eqs. (26)–(29).

Table 2: Properties of Al_2O_3 [8].

Parameters	c_p(J/K)	ρ (kg/m^3)	λ (W/m K)
Value	765	3970	42

3 Numerical solution and model validation

The continuity, momentum, energy and the turbulent equations were solved with the boundary conditions stated above using finite volume software (Open Foam – software for computational fluid dynamics [27]. The semi implicit pressure linked equation (SIMPLE) algorithm was used for pressure-velocity coupling and the second-order upwind scheme was applied to the discretized convection term in the equations [28]. The Gauss-Seidel approach was used to solve the temperature, velocity and turbulent terms. The iterative procedure was programmed to terminate when the convergence criteria are satisfied (the residual for all equations is less than 10^{-6}) [29,30]. A square mesh was used, while the mesh width increased progressively from the wall along the radii direction in order to capture the rapid changes in velocity and temperature that occur at the boundary layer.

3.1 Wall treatment

At the wall, the no-slip condition is applied. This implies that the turbulence quantities ($\bar{u}$, u', k, ε) are equal to zero, but at the near wall region, there is a high variation of these quantities, which is not captured by the k-ε model. As a result, the empirical model's wall function which satisfies the physics of the flow very close to the wall was applied to represent conditions near the wall. The Launder and Splading wall function was used. The range of y^+ value is given as $30 \leq y^+ \leq 300$, where y^+ is the dimensionless normal distance from the wall [31].

3.2 Response surface methodology

Response surface methodology (RSM) is a statistical and mathematical method for building empirical models that will fit the experimental data. The central composite design is one of the methods used in response surface methodology to study the effect of input variables and their interaction on the dependent variables. It is primarily a first-order model augmented with

the additional centre and axial points to provide the extra level required to fit higher-order models. In the RSM method, the multivariate model for the output variable is given as

$$y = \alpha_0 + \sum_{i=1}^{4} \alpha_i x_i + \sum_{i=1}^{4} \alpha_{ii} x_i x_i + \sum_{i=1}^{4} \alpha_{ij} x_i x_j \ , \tag{32}$$

where α_0, α_i, α_{ii}, and α_{ij} are the intercept, linear regression coefficient of the ith factor, quadratic regression coefficient and intercept of the ith and jth factors respectively.

In this study, the effect of four variables: Reynolds number, nanoparticle volume ratio, nanoparticle diameter, entrance temperature and their interactions on the average Nusselt number and pressure drop were estimated. Each factor is set to 5 levels with the alpha value set to 2. Factorial points are located at axial points, while the centre points are located at 0. Based on the number of variables and levels, the condition of 30 runs is defined which consist of 16 factorial points, 8 axial points and 6 centre points. Table 3 shows the variable and the value associated with each level [32–34].

Table 3: Variables and values associated with levels used in response surface methodology.

Variable	Unit	Level				
		-2	-1	0	1	2
Reynolds number, Re		5000	7500	10000	12500	15000
Temperature, T	K	290	300	310	320	330
Diameter, d_p	1×10^{-9} m	20	40	60	80	100
Volume ratio, φ	%	1	2	3	4	5

3.3 Grid dependence and model validation

To check for grid independence, several combinations of grids were used along the radial and axial directions to calculate the average Nusselt number of pure water for Reynolds numbers of 6500. The result is shown in Fig. 2.

Also, the accuracy of the models was validated by comparing the result of the friction factor of water for a range of Reynolds number calculated

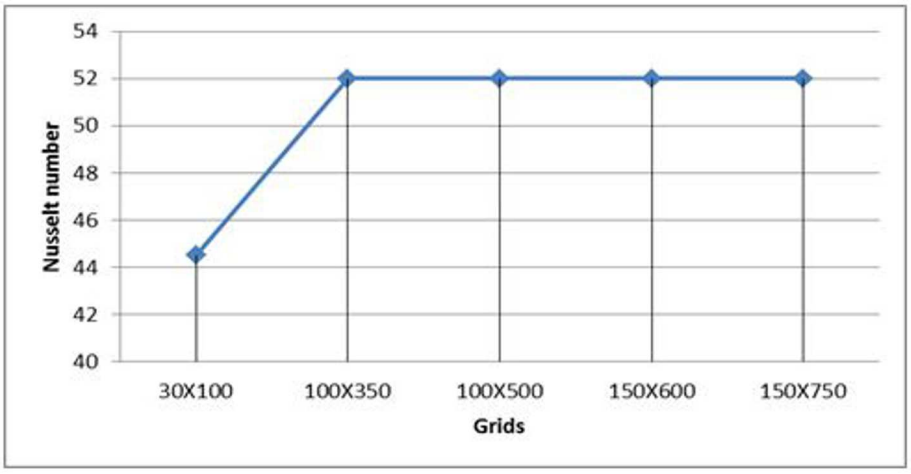

Figure 2: Graph of mean Nusselt number of water at Re = 6500 aganist number of grids.

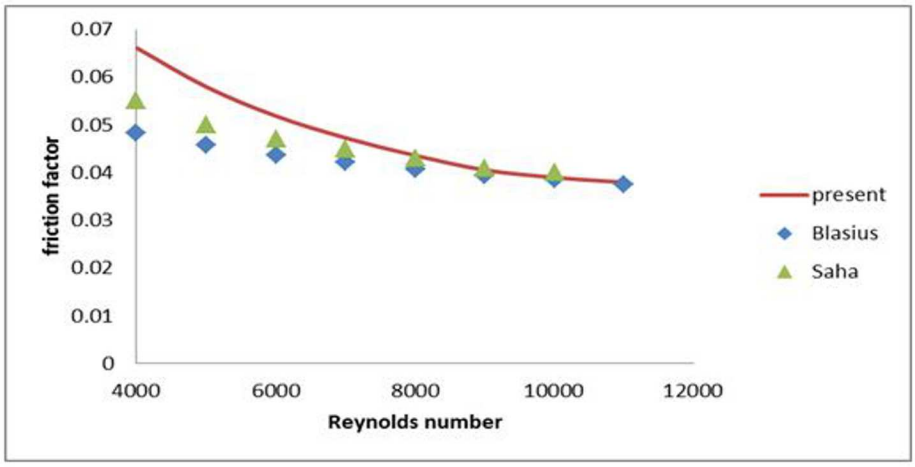

Figure 3: Comparison of friction factor.

from the model using Eq. (11) with the Blasius correlation [35] given by the relation

$$f = \frac{0.316}{\mathrm{Re}^{0.25}}\ , \tag{33}$$

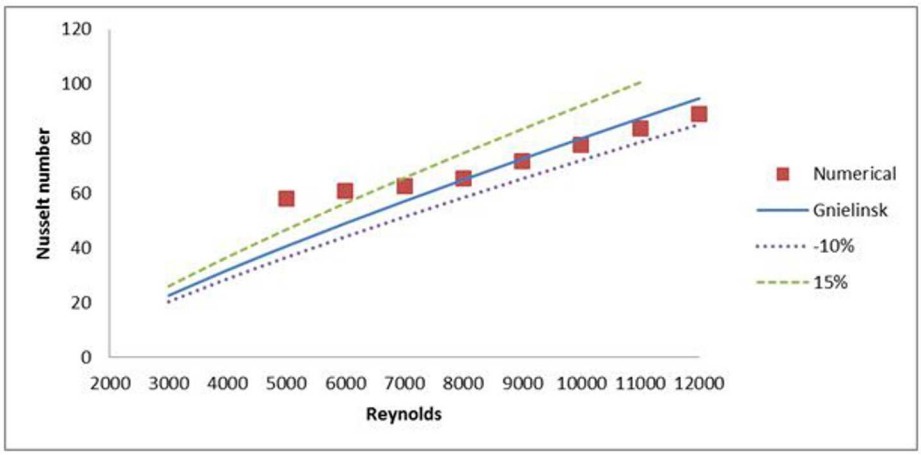

Figure 4: Compariosn of average Nusslet number estimated with Gnielinsk correlation.

where $\mathrm{Re} = \frac{u_{mean} D_h \rho}{\mu}$. The result obtained is shown in Fig. 3 and was found to be consistent with earlier works reported by Saha [9]. Furthermore, the mean Nusselt number estimated using Eq. (14) was compared with the Gnielinski correlation [36] given in

$$\mathrm{Nu} = \frac{\frac{f}{8}\left(\mathrm{Re} - 1000\right)\mathrm{Pr}}{1 + 12.7\left(\frac{\xi}{8}\right)^{0.5}\left(\mathrm{Pr}^{\frac{2}{3}} - 1\right)}\,, \tag{34}$$

where $\mathrm{Pr} = \frac{\mu c_p}{k}$, and $\xi = \left(0.79 \ln \mathrm{Re} - 1.64\right)^{-2}$. The result is shown in Fig. 4. The presented result falls between -10% and 15% of the Gnielinski correlation. It should be mentioned that Eq. (28) is valid for $4.10^3 \leq \mathrm{Re} \leq 10^6$ and $0.5 \leq \mathrm{Pr} \leq 200$.

4 Results and discussion

The effects of four input parameters: Reynolds number, volume ratio, nanoparticle diameter, and entrance temperature of Al_2O_3/H_2O nanofluid flowing through a straight circular pipe in the turbulent regime were investigated on the average Nusselt number and pressure drop. The results of the 30 runs performed with the corresponding Nusselt number and pressure difference are shown in Tab. 4.

Table 4: RSM level of the factors and values of the average Nusselt number and pressure drop.

Run	Re	φ	d_p	T	Nu	Δp
1	-1	-1	-1	-1	60.515	9.948
2	1	-1	1	-1	83.341	18.172
3	-1	1	-1	-1	60.684	14.346
4	1	1	-1	-1	85.474	28.027
5	-1	-1	1	1	59.791	4.239
6	0	0	0	0	68.166	10.619
7	-2	0	0	0	56.474	4.209
8	-1	1	1	1	59.842	5.539
9	1	1	-1	1	76.974	12.766
10	-1	-1	-1	1	59.810	4.534
11	1	-1	-1	-1	83.520	19.436
12	0	0	0	0	68.166	10.619
13	1	1	1	1	76.430	10.821
14	0	0	-2	0	68.577	13.166
15	-1	1	-1	1	59.762	6.534
16	0	0	0	-2	75.887	25.854
17	0	-2	0	0	67.595	8.112
18	-1	-1	1	-1	60.564	9.302
19	0	0	0	0	68.166	10.619
20	0	0	0	0	68.166	10.619
21	1	-1	-1	1	75.872	8.857
22	2	0	0	0	90.044	17.992
23	0	0	2	0	67.949	10.188
24	0	0	0	2	63.387	5.283
25	1	-1	1	1	75.843	8.281
26	1	1	1	-1	84.483	23.758
27	0	0	0	0	68.166	10.619
28	0	2	0	0	68.976	13.747
29	0	0	0	0	68.166	10.619
30	-1	1	1	-1	63.610	6.922

4.1 Nusselt number

Table 5 shows the summary of the model. It reveals that both the linear and quadratic functions are good enough to fit the data, while a polynomial

Table 5. Summary of the model used to fit average Nusslet number.

Model	P-value	R^2	Adj-R^2	Pre-R^2	Dof*	Remark
Linear	< 0.0001	0.9666	0.9612	0.9494	4	–
2FI**	0.1061	0.9798	0.9691	0.9473	6	–
Quadratic	0.0386	0.9893	0.9793	0.9383	4	suggested
Cubic	0.0012	0.9994	0.9974	0.9088	8	aliased
Residual	–	–	–	–	7	–

*Dof – degree of freedom, **2FI – sequential sum of squares for the two-factor interaction

Table 6. Result of ANOVA for mean Nusslet number.

	Sum of square	Degree of freedom	Mean square	F-value	P-value
Model	0.460	4	0.092	338.70	< 0.0001
Reynolds number(A)	0.420	1	0.420	1544.20	< 0.0001
Volume ratio (B)	9.527×10^{-4}	1	9.527×10^{-4}	3.50	0.0735
Temperature (D)	0.031	1	0.031	112.33	< 0.0001
Residual	6.525×10^{-3}	25	2.719×10^{-4}		
Lack of fit	6.525×10^{-3}	20	3.434×10^{-4}		
Pure error	0.000	5	0.000		
Total	0.470	29			

$R^2 = 0.986$, (adj-R^2) – (pre-R^2) = 0.0207, adeq precision = 71.745

above the second degree is not permitted. To verify the accuracy of the model generated and determine the factors that are statistically significant, the analysis of variance (ANOVA) was performed [34]. The summary of ANOVA, after having removed terms with a higher P-value (terms that were not statistically significant) in order to improve the model, is shown in Tab. 5. The result shows that the quadratic model is the best to fit the simulation data. Table 6 shows the result of ANOVA. The model's F- and P-values are 338.7 and < 0.0001, respectively. The model F-value compares the variance of the model to residual's variance, while the P-value measures the probability of obtaining the null hypothesis (none of the input variables has an effect on the Nusselt number and pressure drop). The P-value value which measure the probability of obtaining Null hypothesis and the F-value compares the variance of the model to residual's variance[34]. These values validate that the model is significant from the statistical point of view. It

also reveals that three input variables (Reynolds number, volume ratio and entrance temperature) are statistically significant (note that parameter is statistically significant if it has a P-value less than 0.05). Although, the P-value of volume ratio is greater than 0.05; including it in the model enhances the coefficient of determination – R^2 (which represents how close the simulation data are to the regression line) from a value of 0.92 to 0.986 and thereby justified its inclusion. Furthermore, the difference between the adjusted sum of squares (adj-R^2) and predicted sum of squares (pre-R^2) is 0.0207. The former indicates that 998.6% of the total variance in the mean Nusselt number can be explained by the model, while the latter represents the suitability of the model as its value is less than 0.2.

The regression models obtained for the average Nusselt number is given as

$$\log_e \mathrm{Nu}\,(\mathrm{Re}, \varphi, T,) = 4.23 + 0.13\mathrm{Re} + 0.0063\varphi - 0.036T_{in} \qquad (35)$$

and is valid for: $5000 \leq \mathrm{Re} \leq 15000$; $0.01 \leq \varphi \leq 0.05$; 20 nm$\leq d_p \leq$ 100 nm; 290 K $\leq T \leq$ 330.

4.2 Pressure drop

Table 7. Summary of the model used to fit pressure drop.

Model	P-value	R^2	Adj-R^2	Pre-R^2	dof	Remark
Linear	< 0.0001	0.8698	0.8489	0.8002	4	–
2FI	0.0056	0.9460	0.9175	0.8658	6	–
Quadratic	0.0022	0.9811	0.9635	0.8913	4	suggested
Cubic	0.0047	0.9983	0.9930	0.7551	8	aliased
Residual	–	–	–	–	7	–

Tables 7 and 8 show the model summary and ANOVA results for the pressure drop, respectively. All the input parameters and some interactions between them (Reynolds number-entrance temperature, volume ratio-nanoparticle size and nanoparticle size-entrance temperature) are statistically significant. The F-value of the models is 97.1. This is large enough to validate the suitability of the model. The R^2 value is 0.978 and the difference between the adjusted and predicted R^2 is 0.039. Regression model

Table 8. Result of ANOVA for pressure drop.

	Sum of square	Degree of freedom	Mean square	F-value	P-value
Models	1086.31	9	120.70	97.10	< 0.0001
Reynolds number (A)	386.57	1	386.57	310.97	< 0.0001
Volume ratio (B)	57.71	1	57.71	46.43	< 0.0001
Size (C)	22.76	1	22.76	18.31	0.0004
Temperature (D)	499.42	1	499.42	401.75	< 0.0001
D^2	37.89	1	37.89	30.48	< 0.0001
AB	14.64	1	14.64	11.78	0.0026
AD	52.54	1	52.54	42.27	< 0.0001
BC	8.78	1	8.78	7.06	0.0151
CD	5.99	1	5.99	4.82	0.0401
Residual	24.86	20	1.24		
Lack of fit	24.86	15	1.66		
Pure error	0.00	5	0.00		

$R^2 = 0.9776$, (adj-R^2) – (pre-R^2) = 0.0386, adeq precision = 37.897

for the pressure drop is given as

$$\begin{aligned}\Delta p(\mathrm{Re},\varphi,T,d_p) &= 10.87 + 4.01\mathrm{Re} + 1.55\varphi - 0.974d_p - 4.562T_{in} \\ &+ 1.147T_{in}^2 + 0.957\varphi\mathrm{Re} - 1.812\mathrm{Re}T_{in} \\ &- 0.7408\varphi d_p + 0.612d_pT_{in} \end{aligned} \tag{36}$$

and is valid for $5000 \leq \mathrm{Re} \leq 15000$, $0.01 \leq \varphi \leq 0.05$, 20 nm$\leq d_p \leq$ 100 nm, 290 K$\leq T \leq$ 330 K.

4.3 Test of residual

The test of residual of the model was examined to ascertain the accuracy of the model against noise. Figures 5a and 5b show the normality plots of residual for both the Nusselt number and pressure drop and these indicate the suitability of the models to predict the Nusselt number and pressure drop within the specified range. Also, Figs. 6a and 6b show the plot of the predicted values of Nusselt number and pressure drop against the actual values. The data points are evenly scattered on and around the line, showing that the model gave a good prediction of the Nusselt number and pressure drop.

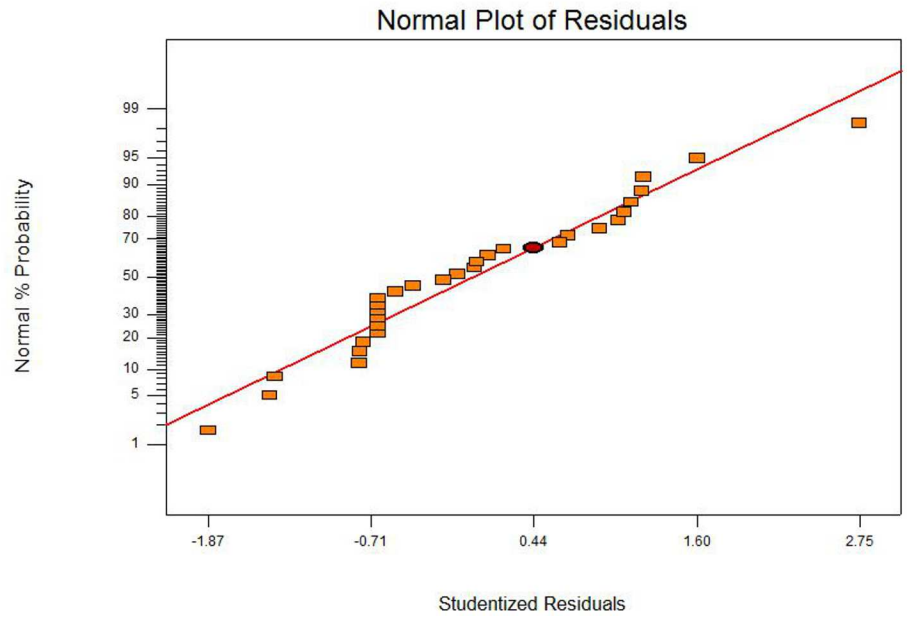

a)

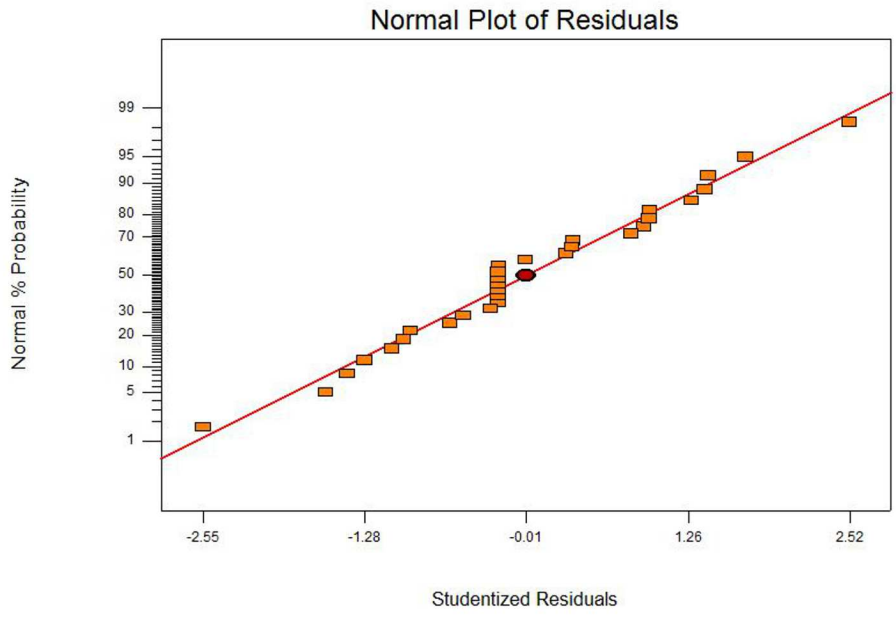

b)

Figure 5: Normal plots of residuals for Nusselt number and pressure drop.

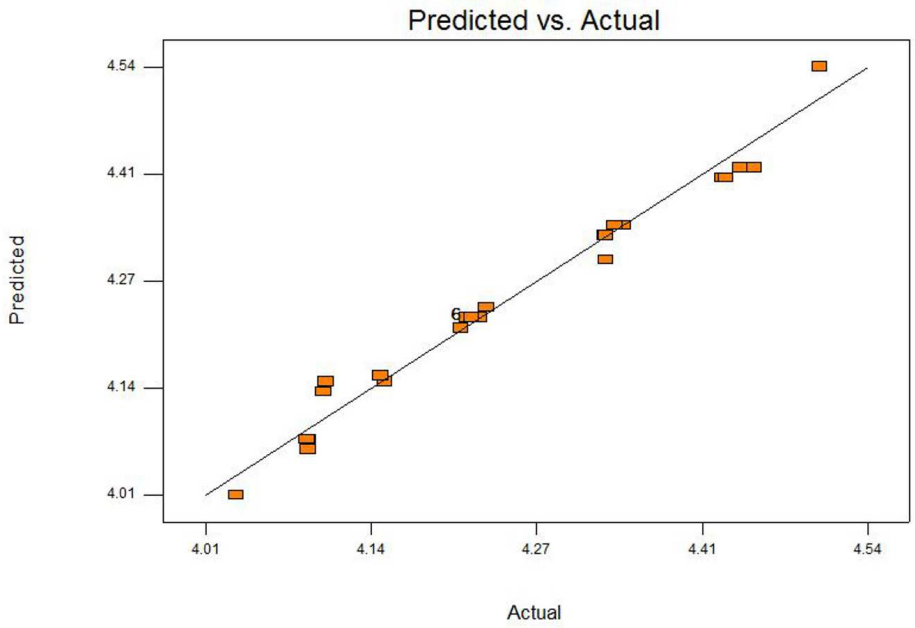

a)

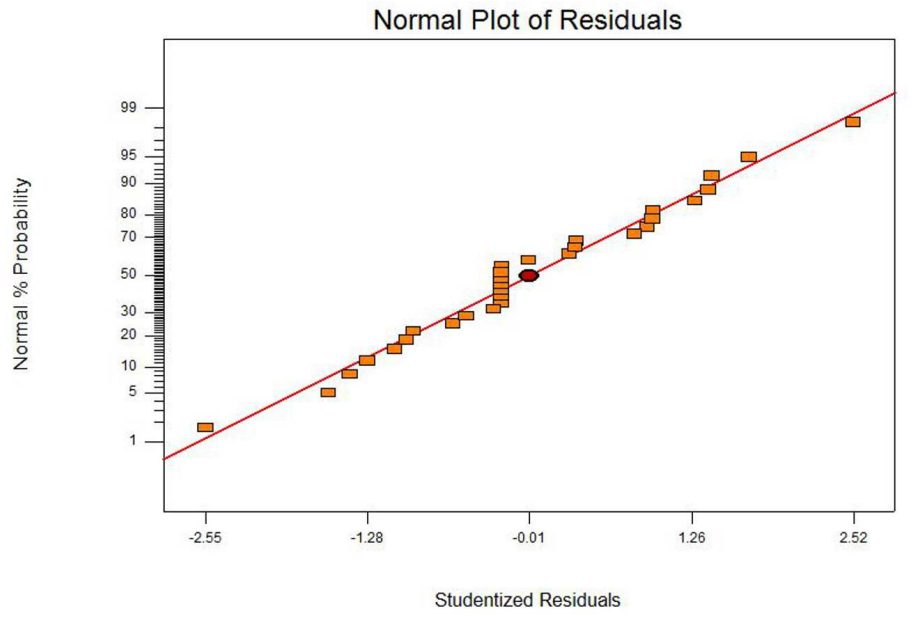

b)

Figure 6: Predicted values of Nusselt number and pressure drop.

4.4 Sensitivity analysis

Sensitivity analysis is a technique used by scientists and engineers to determine how different values of an independent variable affect the observable output variables under a given set of conditions [37–39]. After obtaining the regression model for the observable output it was expedient to carry out a sensitivity analysis to determine the effect of each input parameter on the output variable.

The sensitivity analysis was carried out by taking the partial derivative of the observable output variable with respect to individual input variables. The partial derivative of the regression models for the Nusselt number and pressure drop with respect to the four input parameters are given as:

$$\frac{\partial \mathrm{Nu}}{\partial \mathrm{Re}} = 0.13e^{u} \ , \tag{37}$$

$$\frac{\partial \mathrm{Nu}}{\partial \varphi} = 0.0063e^{u} \ , \tag{38}$$

$$\frac{\partial \mathrm{Nu}}{\partial T_{in}} = -0.036e^{u} \ , \tag{39}$$

$$\frac{\partial \Delta p}{\partial \mathrm{Re}} = 4.013 + 0.9567\varphi - 1.812T_{in} \ , \tag{40}$$

$$\frac{\partial \Delta p}{\partial \varphi} = 1.55 + 0.9567\mathrm{Re} - 0.741T_{in} \tag{41}$$

$$\frac{\partial \Delta p}{\partial d_p} = -0.974 - 0.741\varphi + 0.612T_{in} \tag{42}$$

$$\frac{\partial \Delta p}{\partial T} = -4.562 + 2.29T_{in} - 1.812\mathrm{Re} + 0.612d_p \ , \tag{43}$$

where $u = 4.23 + 0.13\mathrm{Re} + 0.0063\varphi - 0.036T_{in}$.

The positive value of the sensitivity connotes an increment in the observable output variable with respect to increment in the input variable, while a negative value implies the opposite. Tables 9 and 10 show the sensitivity of the input variables against the mean Nusselt number and pressure drop for various configurations. Table 9 shows that for all configurations, both Reynolds number and volume ratio have the positive sensitivities with the highest value for both observed at $(\mathrm{Re} = 2, \varphi = 1, T_{in} = -1)$. The positive sensitivity of Reynolds number and volume ratio implies that an increment in their values will enhance convective heat transfer. This is expected as

an increase in Reynolds number will reduce the thickness of the thermal boundary layer, which in turn enhances convection. Also, an increment in nanoparticle volume ratio will result in an increase in thermal conductivity of the nanofluid. This also enhances convective heat transfer. Table 10 shows that for all configurations Reynolds number has a positive sensitivity with the highest value at $(\mathrm{Re} = -1, \varphi = 0, d_p = 1, T_{in} = -2)$, entrance temperature at $(\mathrm{Re} = 0, \varphi = 1, d_p = -2, T_{in} = -1)$, nanoparticle volume ratio at $(\mathrm{Re} = 2, \varphi = -1, d_p = 0, T_{in} = 1)$ and nanoparticle size at $(\mathrm{Re} = 1, \varphi = 2, d_p = -1, T_{in} = 0)$. Furthermore, it shows that the Reynolds number has a positive sensitivity for all configurations except two cases. This implies that increments in Reynolds number will enhance the pressure drop, which is expected under certain conditions. The positive and the negative sensitivities exhibited by the volume ratio and entrance temperature respectively at some conditions are also expected, as an increment in nanoparticle concentration will enhance the viscosity and this, in turn, would result in an increment in pressure drop. On the other hand, an increment in temperature will cause a decrease in viscosity, which will in turn reduce the pressure drop.

Table 9. Sensitivity analysis of average Nussselt number.

Variables			Sensitivity		
Re	φ	T	Re	φ	T
-2	1	-1	7.2122	0.3329	-1.9972
-1	1	-1	8.1889	0.3779	-2.2677
0	1	-1	9.3164	0.4300	-2.5799
1	1	-1	10.6204	0.4902	-2.9410
2	1	-1	12.1312	0.5599	-3.3594
-1	-2	1	7.4841	0.3454	-2.0725
-1	-1	1	7.5291	0.3475	-2.0850
-1	0	1	7.5744	0.3496	-2.0975
-1	1	1	7.6200	0.3517	-2.1102
-1	2	1	7.6659	0.3538	-2.1229

Table 10. Sensitivity analysis of the rate of pressure drop.

Variables				Sensitivity			
Re	φ	d_p	T	Re	φ	d_p	T
-2	-1	0	1	1.33	-0.37	0.38	1.24
-1	-1	0	1	1.33	0.59	0.38	-0.56
0	-1	0	1	1.33	1.55	0.38	-2.36
1	-1	0	1	1.33	2.51	0.38	-4.16
2	-1	0	1	1.33	3.47	0.38	-5.96
1	-2	-1	0	2.18	3.21	0.51	-6.96
1	-1	-1	0	3.14	3.21	-0.23	-6.96
1	0	-1	0	4.1	3.21	-0.97	-6.96
1	1	-1	0	5.06	3.21	-1.71	-6.96
1	2	-1	0	6.02	3.21	-2.45	-6.96
0	1	-2	-1	6.87	2.95	-2.32	-7.96
0	1	-1	-1	6.87	2.25	-2.32	-7.36
0	1	0	-1	6.87	1.55	-2.32	-6.76
0	1	1	-1	6.87	0.85	-2.32	-6.16
0	1	2	-1	6.87	0.15	-2.32	-5.56
-1	0	1	-2	7.72	-0.11	-2.19	-6.56
-1	0	1	-1	5.91	-0.11	-1.58	-4.36
-1	0	1	0	4.1	-0.11	-0.97	-2.16
-1	0	1	1	2.29	-0.11	-0.36	0.04
-1	0	1	2	0.48	-0.11	0.25	2.24

5 Conclusion

The convective heat transfer and pressure drop of Al_2O_3/H_2O nanofluid in turbulent flow through a straight circular pipe were investigated using the single-phase model. The numerical investigation was carried out to study the effect of four parameters – the Reynolds number, volume ratio, nanoparticle size and the entrance temperature on the heat transfer performance and pressure drop. The central composite design method was used for the response surface methodology (RSM). Based on the number of variables and levels, the condition of 30 runs was defined. The analysis of variance (ANOVA) was performed to determine the parameters that are

statistically significant. The results showed that all the input variables were statistically significant to the pressure drop, while three of them were significant to convective heat transfer. Furthermore, sensitivities analysis was performed on the regression models generated for both the mean Nusselt number and pressure drop. The results obtained are summarized below:

- Increasing the Reynolds number and volume ratio of the nanoparticles enhances the convective heat transfer when $d_p = -1$ and $T_{in} = 0$.
- The most sensitive parameter to convective heat transfer is the Reynolds number.
- Increasing the Reynolds number and volume ratio enhances the pressure drop when ($d_p = -1$ and $T_{in} = 0$).
- For most of configurations considered, an increase in entrance temperature suppresses pressure drop except at 3 configurations listed below: Re $= -1$, $\varphi = 0$, $d_p = 1$, $T_{in} = 1$; Re $= -1$, $\varphi = 0$, $d_p = 1$, $T_{in} = 2$ and Re $= -2$, $\varphi = -1$, $d_p = 0$, $T_{in} = 1$.

Received 23 April 2018

References

[1] Choi S.U.S.: *Enhancing thermal conductivity of fluids with nanoparticles.* In: Developments and Applications of Non-Newtonian Flows (D.A. Siginer, H.P. Wang, Eds.). ASME FED-Vol.2 31/MD-Vol. 66, New York 1995, 99–105.

[2] Eastman J.A., Choi S.U.S., Li S., Yu W., Thompson L.J.: *Anomalously increased effective thermal conductivities of ethylene glycol-based nanofluids containing copper nanoparticles.* Appl. Phys. Lett. **78**(2001), 6, 718–720.

[3] Wang X.Q., Mujumdar A.S.: *Heat transfer characteristics of nanofluids: A review.* Int. J. Therm. Sci. **46**(2007), 1, 1–19.

[4] Fadodun O.G, Amosun A.A; Okoli N.L., Olaloye D.O, Durodola S.S and Ogundeji J.A.: *Sensitivity analysis of entropy production in Al_2O_3/H_2O nanofluid through converging pipe.* J. Therm. Anal. Calorim. **12**(2019), 12, 1–14.

[5] Sharma K.V., Sundar L.S., Sarma P.K.: *Estimation of heat transfer coefficient and friction factor in the transition flow with low volume concentration of Al_2O_3 nanofluid flowing in a circular tube and with twisted tape insert.* Int. Commun. Heat Mass **36**(2009), 5, 503–507.

[6] Chandrasekar M., Suresh S., Bose A.C.: *Experimental studies on heat transfer and friction factor characteristics of Al2O3/water nanofluid in a circular pipe under transition flow with wire coil inserts.* J. Heat Transfer Eng. **32**(2011), 6, 485–496.

[7] Li Q., Xuan Y.: *Convective heat transfer and flow characteristics of Cu-water nanofluid*. Science in China E: Technol. Sci. **45**(2002), 4, 408–416.

[8] Shanbedi M., Jafari D., Amiri A., Harris S.Z., Baniadam M.: *Prediction of temperature performance of a two-phase closed thermosyphon using artificial neural network*. Heat Mass Transfer **49**(2013), 1, 65–73.

[9] Saha G., Paul M.C.: *Numerical analysis of the heat transfer behaviour of water-based Al2O3 and TiO2 nanofluids in a circular pipe under the turbulent flow condition*. Int. Commun. Heat Mass **56**(2014), 96–108.

[10] Safaei M.R., Ahmadi G., Goodarzi M.S., Safdari S.M., Goshayeshi H.R., Dahari M.: *Heat transfer and pressure drop in fully developed turbulent flows of graphene nanoplatelets-silver/water nanofluids*. Fluids **1**(2016), 3, 20.

[11] Hussein A.M., Bakar R.A., Kadirgama K., Sharma, K.V.: *Simulation study of turbulent convective heat transfer enhancement in heated tube flow using TiO2-water nanofluid*. IOP Conf. Ser.: Materials Science and Engineering. **50**(2013), 1.

[12] Fadodun O.G., Amosun A.A., Ogundeji J.A., Olaloye D.O.: *Numerical investigation of thermal efficiency and pumping power of Al_2O_3/H_2O nanofluid in pipe using response surface methodology.* J. Nanofluids **8**(2019), N0 7, 1566-1576.

[13] Fadodun O.G., Amosun A.A., Salau O.A., Ogundeji J.A., Olaloye D.O.: *Numerical investigation of thermal performance of single-walled carbon nanotube nanofluid under turbulent flow conditions.* Eng. Rep. **1**(2019).

[14] Chan J.S., Ghadimi A., Simon H., Metselaar C., Lotfizadehdehkordi B.: *Optimization of temperature and velocity on heat transfer enhancement of non-aqueous alumina nanofluid*. J. Eng. Sci. Technology **10**(2015), 85–101.

[15] Albojamal A., Vafai K.: *Analysis of single phase, discrete and mixture models, in predicting nanofluid transport*. Int. J. Heat Mass **114**(2017), 225–237.

[16] Zhang Y., Zhang H., Yu H., Ma C.: *Response surface methodology control rod position optimization of a pressurized water reactor core considering both high safety and low energy dissipation*. Entropy **19**(2017), 2, 63.

[17] Mamourian M., Shirvan K.M., Mirzakhanlari S.: *Two phase simulation and sensitivity analysis of effective parameters on turbulent combined heat transfer and pressure drop in a solar heat exchanger filled with nanofluid by response surface methodology*. Energy **109**(2016), 49–61.

[18] Wen J., Li K., Zhang X., Wang C., Wang S., Tu J.: *Optimization investigation on configuration parameters of serrated fin in plate-fin heat exchanger based on fluid structure interaction analysis*. Int. J. Heat Mass **119**(2018), 1, 282–294.

[19] Shanbedi M., Zeinali H.S., Maskooki A., Eshghi H.: *Statistical analysis of laminar convective heat transfer of MWCNT-deionized water nanofluid using the response surface methodology*. Num. Heat Transfer A-Appl. **68**(2015), 4, 454–469.

[20] Konchada P.K., Vinay P.V. and Bhemuni V.: *Statistical analysis of entropy generation in longitudinally finned tube heat exchanger with shell side nanofluid by a single phase approach*. Arch. Thermodyn. **37**(2016), No. 3, 3-22.

[21] Kazemi A, Azizi H.H., Zeinali S.: *Prediction of stability and thermal conductivity of SnO_2 nanofluid via statistical method and an artificial neural network*. Braz. J. Chem. Eng. **32**(2015), 4, 903–917.

[22] Salman B.H., Mohammed H.A., Kherbeet A.: *Numerical study of three different approaches to simulate nanofluids flow and heat transfer in a microtube.* Heat Transfer – Asian Res. **45**(2016), 1, 46–58.

[23] Versteeg H.K., Malalasekera W.: *An Introduction to Computational Fluid Dynamics: The Finite Volume Method.* Pearson Education, 2007.

[24] Kays W.M., Crawford M., Weigang B.: *Convective Heat and Mass Transfer.* Tata McGraw-Hill Education, India 2012.

[25] Buongiorno J.: *Convective transport in nanofluids.* J. Heat Transf. **128**(2006), 3, 240–250.

[26] Corcione M.: *Empirical correlating equations for predicting the effective thermal conductivity and dynamic viscosity of nanofluids.* Energ. Convers. Manage.**52**(2011), 1, 789–793.

[27] Greenshields C.J.: *OpenFOAM User Guide Version 4.0.* OpenFOAM Foundation Ltd., London 2016.

[28] Nadila N.I., Lazim T.M., Mat S.: *Verification of heat transfer enhancement in tube with spiral corrugation.* AIP Conf. Proc. **2062**(2019), 1, 020032-1-6.

[29] Andreozzi A., Manca O., Nardini S., Ricci D.: *Forced convection enhancement in channels with transversal ribs and nanofluids.* Appl. Therm. Eng. **98**(2016), 1, 1044–1053.

[30] Khan A.Q., Rasheed A.: *Mixed Convection Magnetohydrodynamics Flow of a Nanofluid with Heat Transfer: A Numerical Study.* Math. Probl. Eng. **2019**(2019), 1 – 14.

[31] Launder B.E. and Spalding D.B.: *The numerical computation of turbulent flows.* Comput. Meth. Appl. bf 3(1974), 2, 269–289..

[32] Farhad F., Dariush K., Mojtaba M.: *Optimization of double pipe heat exchanger with response surface methodology using nanofluid and twisted tape.* Fluid Mech. **3(**2017), 3, 20–28.

[33] Rashidi S., Bovand M., Esfahani J.A.: *Sensitivity analysis for entropy generation in porous solar heat exchangers by RSM.* J. Thermophys. Heat Tr. **31**(2016), 2, 390-402.

[34] Carley K.M., Kamneva N.Y., Reminga J.:*Response surface methodology.* CASOS Techn. Rep. CMU-ISRI-04-136. Carnegie-Mellon Univ Pittsburgh 2004.

[35] Blasius H.: *Das Aehnlichkeitsgesetz bei Reibungsvorgängen in Flüssigkeiten*, Mitteilungen über Forschungsarbeiten auf dem Gebiete des Ingenieurwesens **131**(1913), 3, 1-41 (in German).

[36] Gnielinski V.:*New equations for heat and mass transfer in turbulent pipe and channel flow.* Int. Chem. Eng. **16**(1976), 1 359–368.

[37] Campolongo F., Braddock R.: *The use of graph theory in sensitivity analysis of model output: a second order screening method.* Reliab. Eng. Syst. Saf. **64**(1999), 1, 1–12.

[38] Griewank A., Walther A.: *Evaluating derivatives: principles and techniques of algorithmic differentiation.* SIAM, Philadelphia 2008.

[39] Fadodun O.G., Ayodeji O.S., Adebimpe A.A., Francis I.I.: *Sensitivity analysis and evaluation of critical size of reactor using response surface methodology.* Int. J. Emerging Technol. **10**(2019), 4, 184–190.